Analysis and Prediction of Ocean Swell Using Instrumented Buoys

THEODORE METTLACH AND DAVID WANG

Applied Technology Division, Computer Sciences Corporation, Stennis Space Center, Mississippi

PAUL WITTMANN

Ocean Models Division, Fleet Numerical Oceanography Center, Monterey, California

(Manuscript received 14 January 1993, in final form 4 June 1993)

ABSTRACT

During the period 20–23 September 1990, the remnants of Supertyphoon Flo moved into the central North Pacific Ocean with sustained wind speeds of 28 m s^{-1}. The strong wind and large fetch area associated with this storm generated long-period swell that propagated to the west coast of North America. National Data Buoy Center moored-buoy stations, located in a network that ranged from the Gulf of Alaska to the California Bight, provided wave spectral estimates of the swell from this storm. The greatest dominant wave periods measured were approximately 20–25 s, and significant wave heights measured ranged from 3 to 8 m. Wave spectra from an array of three nondirectional buoys are used to find the source of the long-period swell. Directional wave spectra from a heave–pitch–roll buoy are also used to make an independent estimate of the source of the swell. The ridge-line method, using time-frequency contour plots of wave spectral energy density, is used to determine the time of swell generation, which is used with the appropriate surface pressure analysis to infer the swell generation area. The diagnosed sources of the swell are also compared with nowcasts from the Global Spectral Ocean Wave Model of the Fleet Numerical Oceanography Center. A simple method of predicting the propagation of ocean swell, by applying a simple kinematic model of wave propagation to the estimated point and time source, is demonstrated.

1. Introduction

The network of National Data Buoy Center (NDBC) buoys along the west coast of North America has grown steadily to over 20 stations in the past 20 years. Using wave spectra obtained from these buoys, it is now feasible to identify, track, and predict the movement of high-height, long-period waves from far-off storms. The motivation for developing such a capability is based on the general need to accurately forecast the arrival of potentially damaging high-height, long-period swell. Such swell can adversely affect human marine activities—offshore operations, marine navigation, and commercial and recreational activities in coastal waters. Horrer (1948) described the extensive damage at Long Beach, California, in April 1930 from 20-s period swell that originated from a storm in the Southern Ocean and from 16-s period swell in September 1939 that originated from a tropical storm west of Mexico. Such swell can be very dangerous. Liang (1990) described the tragic consequences of such waves on the unsuspecting. In October 1987 nine elementary school children were drowned by sudden typhoon-generated swell hitting the Mau-Pi-Tou coast of Taiwan. The typhoon was 600 km offshore, was moving away from Taiwan, and the weather service had recently downgraded the intensity of the storm from *strong* to *moderate*. Damage can be minimized and injury averted with adequate warning of approaching high swell.

Two studies have demonstrated the value of the NDBC network in identifying long-period swell situations. Earle et al. (1984) used eight NDBC buoys along the west coast of North America to quantitatively identify high swell propagating from along the Oregon and Washington coasts southward to the coast of southern California. Hamilton (1992) documented the measurement by 19 NDBC stations and six Canadian buoys of long-period low-amplitude swell along the east coast of North America that had been generated from a storm in the southern Atlantic Ocean. In these studies the sources of the swell were determined in two steps. First, the distance to the generation area from a buoy was found by relating the difference in time between the onset of swell energy at two frequencies to the theoretical dispersion of surface gravity waves. Then, the appropriate meteorological charts were inspected for any storms at the calculated distance that would have generated the detected swell waves. While this can be

Corresponding author address: Mr. Theodore Mettlach, Building 3203, Computer Sciences Corporation, Applied Technology Division, Stennis Space Center, MS 39529-6000.

a very effective method for identifying swell origin and forecasting swell propagation, it cannot be easily automated.

Other investigators have estimated the origin of swell by finding both the distance and the azimuth to the generation area. Munk et al. (1963) used an array of three bottom-mounted pressure transducers off San Clemente Island, California, to derive directional and nondirectional wave spectra and then from those spectra determine the time, distance, and direction of swell generated by several distant storms in the Pacific Ocean and Indian Ocean. Snodgrass et al. (1966) used a pair of bottom-mounted pressure transducers located off Honolulu, Hawaii, to detect the source of several swell events during a 2.5-month period. In principle, directional arrays can be used to identify the origin of swell and, thus, to forecast further propagation past the measuring array. However, the sensors used in both of these studies were located very near shore, thereby precluding their use for swell warning.

González et al. (1987) have demonstrated that the age and source of ocean swell from a hurricane can be determined from observations made with a spaceborne synthetic aperture radar (SAR) and a simple kinematic model of wave propagation. During the second Shuttle Imaging Radar Experiment (SIR-B), 1.5 min of SAR imagery near Hurricane Josephine were acquired and used to show how swell waves radiate outward from a tropical cyclone. While there can be no doubt that the extended perspective from elevated space platforms holds great promise for the capability to completely describe the spectral characteristics of the entire two-dimensional sea surface, spaceborne systems are vastly more expensive than in situ sensors.

Others have studied swell propagation using measurements from heave–pitch–roll buoys in deep water. Gjevik et al. (1988) used directional wave spectra from eight heave–pitch–roll buoys to study long-period swell wave events on the Norwegian shelf. Wang and Carolan (1991) used a 3-m-diameter NDBC heave–pitch–roll buoy, moored in Monterey Bay off the coast of California, to estimate the azimuth to and the time of the origin of high swell generated by a storm in the Gulf of Alaska. Heave–pitch–roll buoys have the capability of providing valuable information for determining the origin of swell, but such systems are relatively expensive.

The purpose of this paper is to demonstrate how wave spectra from NDBC moored-buoy stations can be applied to three related, but different, methods for determining the origin of ocean swell, and thus provide the necessary information to forecast the propagation of that swell. The first method uses the wave spectra from pairs of nondirectional buoy stations located far apart. A *nondirectional buoy,* throughout this paper, shall refer to a buoy that is limited to only measurements of vertical acceleration, which can be used to find surface-displacement spectra. Such spectra will be referred to as nondirectional wave spectra. While this method is based on well-established theories of wave propagation, it has never been practically demonstrated using NDBC buoy data. The results of this method are compared to the results from the second method, which uses directional wave information derived from an NDBC directional buoy. Throughout this paper a *directional buoy* shall refer to a heave–pitch–roll buoy that provides surface-displacement spectra, and directional spectra. The estimates of swell origin inferred from the directional and nondirectional buoy methods are also compared to the third method for finding swell origin, which uses ridge-line depictions employed by Munk et al. (1963), as well as the appropriate synoptic weather charts and linear wave theory.

In September 1990 the extratropical remnants of Supertyphoon Flo produced high-height, long-period swell that radiated outward from the wave generation area in the central North Pacific Ocean and were detected by 18 operational NDBC buoys along the west coast of North America, providing an ideal case for studying swell propagation. The response of all 18 buoys to this swell is documented. The spectral wave estimates from three buoys are used to demonstrate the applicability of the three different methods for identifying the time and location of swell generation. The estimates of the time and location of swell generation are also compared with the corresponding analyses from the Global Spectral Ocean Wave Model (GSOWM) of the Fleet Numerical Oceanography Center (FNOC), Monterey, California. It is shown that with the current NDBC network of buoys, it is feasible to implement these methods for identifying the source of swell for the ultimate goal of forecasting high-swell events along the west coast of the United States.

2. The evolution of Supertyphoon Flo

Supertyphoon Flo was the fourth of six western Pacific tropical cyclones in September 1990 and the first of four supertyphoons for the year. On 16 September Typhoon Flo reached supertyphoon intensity with sustained winds in excess of 67 m s^{-1} as it passed about 925 km east of Taiwan. It was the most powerful typhoon to hit Honshu, Japan, in 19 years. Thirty-eight people were reported dead or missing as a result of the strong winds and flooding associated with this storm.

The final warning from the Joint Typhoon Warning Center, Guam, was issued on 20 September. At that time the storm was located near 37.9°N, 139.8°E, had sustained winds of 28 m s^{-1}, and had a central pressure of 980 hPa (Joint Typhoon Warning Center 1990). The storm weakened during the next 12 h but then reintensified on 21 September into a major extratropical cyclone. On 22 September the storm reached maximum intensity with a central pressure of 968 hPa, near 47.5°N, 180.0°. For the next 36 h the storm dom-

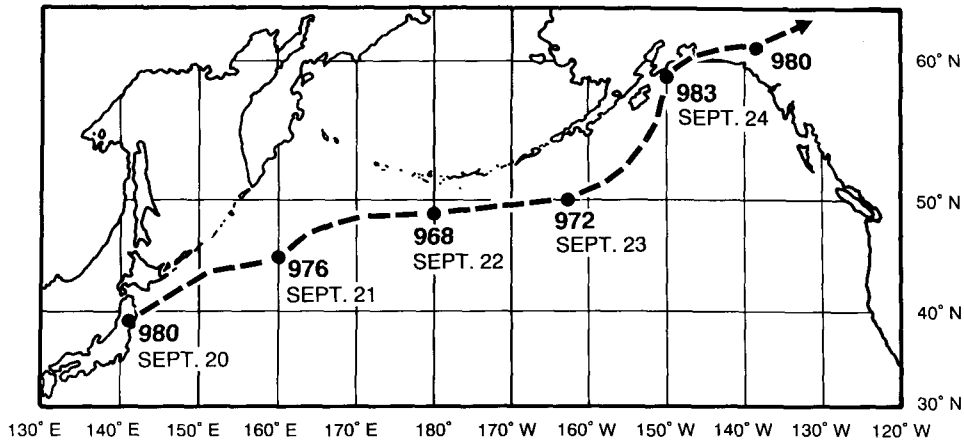

FIG. 1. The path of Supertyphoon Flo and its extratropical remnants through the central Pacific. The central pressure (hPa) of the storm at 0000 UTC of each day are denoted.

inated the weather of the central North Pacific Ocean. Figure 1 shows the path of the storm from the time of its tropical-to-extratropical transition until its dissipation in the Gulf of Alaska on 24 September.

Two to three days after the time of maximum storm intensity, the NDBC moored buoys that were located along the west coast of North America and in the open waters of the northeast Pacific Ocean detected long-period swell of moderate to high height from this storm.

3. Wave measurements

The 18 moored-buoy stations used for this study are listed in Table 1 by World Meteorological Organization station location number, hull type, and water depth. Figure 2 shows the geographical position of each station used. The nondirectional wave measurement system on each buoy, except station 46042, consisted of a strapped-down accelerometer (with its measurement axis perpendicular to the buoy deck) and an on-board data processor. The details of the data collection and analysis procedures for the NDBC nondirectional wave system is best described by Steele and Earle (1979). Each hour (generally from minute 30 to minute 50 or from minute 29 to minute 49, depending on the on-board data processor used) a 20-min record of quasi-vertical hull accelerations, sampled at a rate of 1 Hz, is collected. An acceleration spectrum is produced using a segmented fast Fourier transform (FFT), performed on 100-s windowed sections, overlapped by 50 s. Wave spectral estimators are obtained from the acceleration spectral estimators by dividing the acceleration energy in each frequency band by the radian band center frequency to the fourth power. Displacement spectral estimators are obtained for frequencies ranging from 0.03 to 0.40 Hz in intervals of 0.01 Hz. Each estimator is produced with approximately 33 degrees of freedom. The wave spectrum $S(f)$ is used to compute the significant wave height by

$$H_s = 4\left[\int_{0.03\ \mathrm{Hz}}^{0.40\ \mathrm{Hz}} S(f)df\right]^{1/2}.$$

The dominant wave period is the wave period corresponding to the center frequency of the frequency band with the maximum nondirectional spectral density.

In addition to the surface-displacement spectrum, station 46042 reported directional wave data nearly each hour during this event. The method developed by NDBC to estimate directional wave information

TABLE 1. Station information. There are seven different hulls used by NDBC: 12D (12-m discus), 10D (10-m discus), 6N (6-m naval oceanographic meterological automated device—NOMAD), 3D (3-m discus), LNB (U.S. Coast Guard 12-m discus large navigational buoy), ELB (U.S. Coast Guard 2.7-m exposed location buoy), and 2D (2.3-m foam-discus-hulled coastal buoy). Descriptions of the NDBC buoy hulls are given by Hamiltion (1990).

Station	Latitude (°N)	Longitude (°W)	Hull type	Water depth (m)
46003	51.85	155.92	6N	4709
46001	56.47	148.18	6N	4206
46006	40.81	137.65	12D	3932
46002	42.53	130.25	6N	3420
46041	47.42	124.53	3D	44
46046	46.33	124.18	2D	33
46010	46.18	124.17	LNB	60
46040	44.78	124.30	3D	112
46027	41.84	124.40	ELB	57
46022	40.75	124.50	3D	250
46030	40.44	124.50	ELB	57
46014	39.22	123.98	10D	371
46013	38.23	123.30	10D	125
46026	37.75	122.68	LNB	33
46012	37.39	122.72	3D	92
46042	36.75	122.40	3D	2103
46011	34.88	120.87	3D	201
46023	34.25	120.65	3D	600

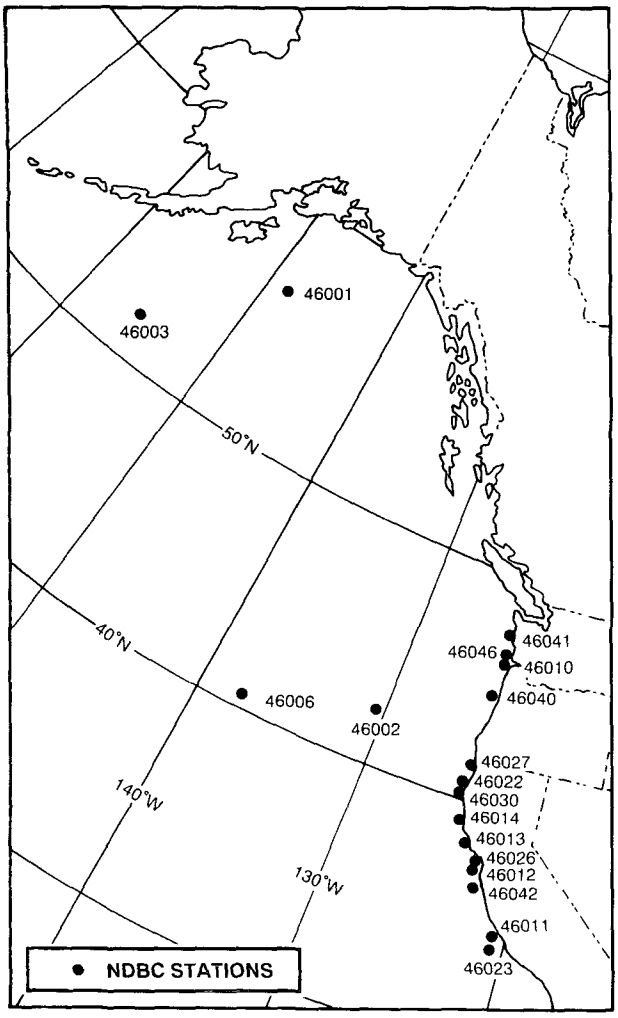

FIG. 2. The location of the NDBC stations. The five-digit number of each buoy location is its WMO station identifier.

from a heave–pitch–roll (directional) buoy is based on the approach of Longuet-Higgins et al. (1963). The details of the NDBC directional measurement system and the computation of directional wave spectra are described by Steele et al. (1985, 1992). The heave–pitch–roll sensor on station 46042 is a Datawell Hippy 40 Mark II. Records of heave, pitch, and roll, sampled at a frequency of 1 Hz, are acquired each hour from minute 24 to minute 44. Pitch and roll motions are converted into north–south and east–west buoy slopes using the azimuth of the buoy bow. Buoy azimuth is computed from the two orthogonal magnetic field components parallel to the buoy bow and starboard beam, measured by an on-board triaxial magnetometer. The six co- and two-quadrature spectra related to the hull surface displacement and slope records, covering the frequency range from 0.03 to 0.35 Hz in intervals of 0.01 Hz, are computed by an on-board processor.

The directional spectrum $E(f, \theta)$ expressed as a Fourier series expansion,

$$E(f, \theta) = \frac{a_0}{2} + (a_1 \cos\theta + b_1 \sin\theta) + (a_2 \cos 2\theta + b_2 \sin 2\theta) + \cdots,$$

can be rewritten as the product of $S(f)$ and the directional distribution function $D(f, \theta)$ or

$$E(f, \theta) = S(f)D(f, \theta),$$

where

$$\int_0^{2\pi} D(f, \theta)d\theta = 1.$$

NDBC directional buoys produce only estimates of the first two harmonic terms in the Fourier series expansion; therefore, $D(f, \theta)$ can be expressed as

$$D(f, \theta) \approx \frac{1}{\pi}\left[\frac{1}{2} + \rho_1 \cos(\theta - \theta_1) + \rho_2 \cos 2(\theta - \theta_2)\right]$$

(Steele et al. 1985).

The angles θ_1 and θ_2 are the two frequency-dependent wave directions measured clockwise from north around to the direction the wave is coming from. The angle θ_1 is usually referred to as the mean wave direction:

$$\theta_1 = \left(\frac{3\pi}{2}\right) - \tan^{-1}(b_1, a_1).$$

The angle θ_2 is usually referred to as the principle wave direction and is defined as

$$\theta_2 = \left(\frac{3\pi}{2}\right) - \left(\frac{1}{2}\right)\tan^{-1}(b_2, a_2).$$

Two frequency-dependent directional spreading parameters, ρ_1 and ρ_2, are defined, respectively, as follows:

$$\rho_1 = \frac{(a_1^2 + b_1^2)^{1/2}}{a_0},$$

and

$$\rho_2 = \frac{(a_2^2 + b_2^2)^{1/2}}{a_0}.$$

The Fourier coefficients, a_0, a_1, b_1, a_2, and b_2 can be computed from the co- and two-quadrature spectra of buoy heave, buoy east–west slope, and buoy north–south slope (Longuet-Higgins et al. 1963).

Both directional and nondirectional wave analysis results from NDBC buoys are transmitted to the National Weather Service Telecommunications Gateway, Silver Spring, Maryland, via the Geostationary Operational Environmental Satellite (GOES) within minutes of data acquisition and on-board processing. Shoreside processing includes correcting spectra for filter acquisition and on-board processing. Shoreside

processing includes correcting spectra for filter responses during signal conditioning and for particular buoy hull responses to moorings and higher-frequency wave energy. The buoy hull types used by NDBC do not follow waves perfectly at all frequencies, either because of the size of the buoy in relation to the wavelengths present or because of the mooring attached to the hull constraining the buoy's motion or both. NDBC has developed a mathematical algorithm to correct for sensor and hull-mooring responses automatically each hour in the calculation of the Fourier coefficients (Steele et al. 1992). Unlike the surface-displacement (nondirectional) spectra obtained from the vertically stabilized accelerometer of the Datawell Hippy 40, those from nondirectional buoys must be corrected for small levels of excess low-frequency energy noise caused by strapping down the accelerometer (Hamilton 1992). Shoreside processing for all stations is generally completed within 1 h. The timeliness of the wave analysis results from NDBC offshore ocean stations makes it possible to recognize incoming swell hours before its arrival at the coast.

4. NDBC wave estimates: 22–29 September 1990

The time series of significant wave height and dominant wave period for the 18 stations used in this study,

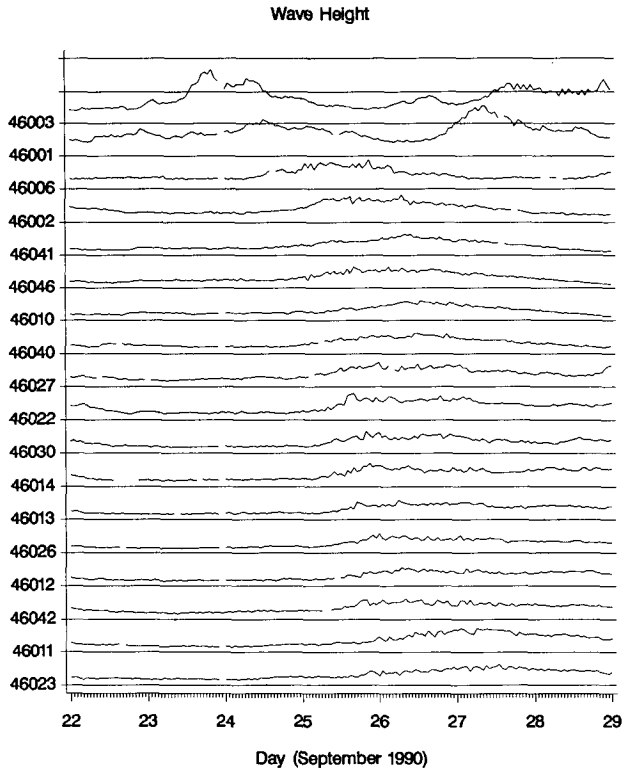

FIG. 3. Time series of significant wave height (m) at each station from 22 to 29 September 1990. The distance between horizontal lines represents 5 m. The individual ordinates run from 0 to 5 m except for the additional 5 m for station 46003.

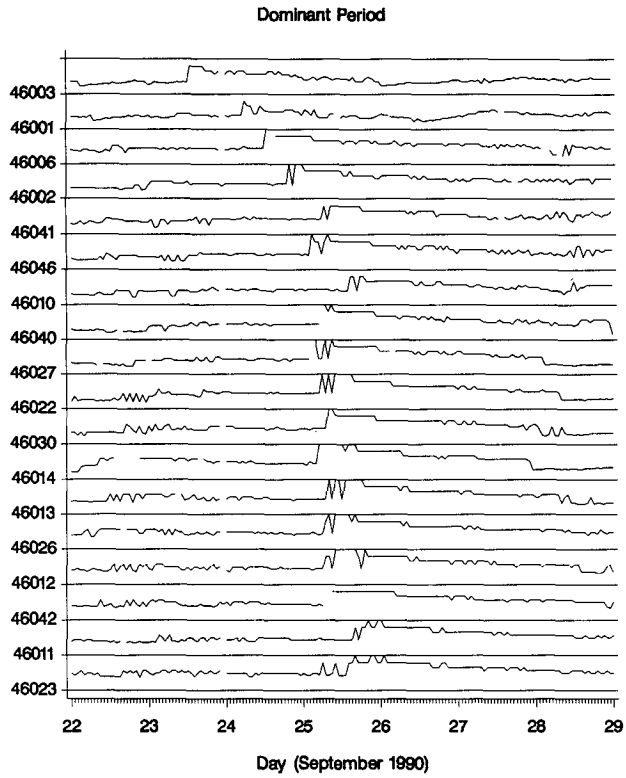

FIG. 4. Time series of dominant period (s) at each stations from 22 to 29 September 1990. The distance between horizontal lines represents an interval from 0 to 25 s.

shown in Figs. 3 and 4, respectively, reveal high- to moderate-height, long-period waves arriving at each of the stations from 23 to 25 September. Significant wave heights increased from 1 to 3 m at several stations. The leading edge of the swell energy is very noticeable from the changes in dominant wave period. Dominant wave periods increased rapidly from 10 to 25 s in 1–2 h at more than half of the stations. The dominant wave period plots are somewhat *jumpy* because of the 0.01-Hz resolution of the frequency bands.

Time series of the wave spectral density for frequencies 0.04, 0.05, and 0.06 Hz are shown in Figs. 5a–c, respectively. The greatest energy was detected at the first station affected, station 46003, south of the Aleutian Islands. The next station to be affected was station 46001, in the Gulf of Alaska, approximately 670 km northeast of station 46003.

These time series represent the coherent arrivals of long-period swell from a distant storm. The onset of swell energy within the NDBC network occurred over a relatively short time period. At many stations there was little, if any, local wind during the onset of this wave energy. The extent of the swell arrival is clearly visible by the onset of swell energy from Cape Elizabeth, Washington, to Point Conception, California, that occurred in approximately 12 h. In general, the stations with the greater amounts of wave energy were those

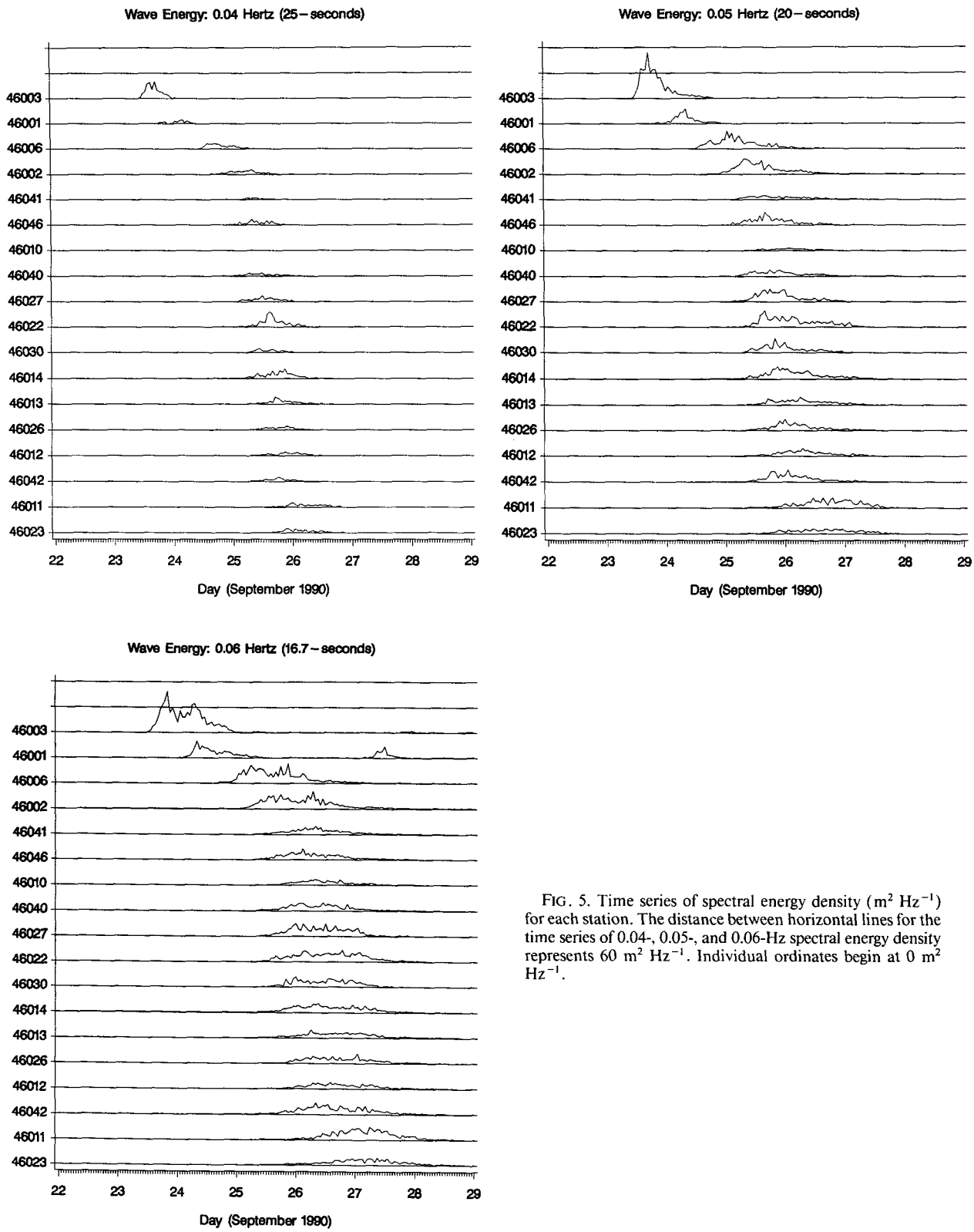

FIG. 5. Time series of spectral energy density (m^2 Hz^{-1}) for each station. The distance between horizontal lines for the time series of 0.04-, 0.05-, and 0.06-Hz spectral energy density represents 60 m^2 Hz^{-1}. Individual ordinates begin at 0 m^2 Hz^{-1}.

located farther west and north, and, therefore, closer to the wave generation source.

Although the wave energies at each station depicted in Figs. 5a–c clearly show a marked increase, there is noticeable variability from hour to hour at some stations as well as variability from station to station. There was significantly less 0.04- and 0.05-Hz energy density at stations 46041 (Cape Elizabeth, Washington) and 46010 (Columbia River, Oregon) than at 46046 (Cape Disappointment, Washington) and 46040 (Cape Foulweather, Oregon). These differences are significant and will be discussed further.

5. Determination of wave generation area using nondirectional wave spectra—Technique

The location and the time of the generation of the wave energy detected by the NDBC buoys on 24–25 September were found by applying linear wave theory. Swell waves suffer little molecular viscous dissipation and the level of turbulence in the ocean does not affect their propagation significantly (Khandekar 1989). Snodgrass et al. (1966) have shown that swells seem to obey the linear wave theory of propagation and do not seem to be affected by propagation through zones of steady wind. It is assumed that the waves originate from nearly a point source or a generation region sufficiently far away to be considered as nearly a point source.

The time of wave generation, t_o, can be found by measuring the times that waves of different frequencies arrive at a station. Wave energy travels along great-circle routes at the frequency-dependent group velocity,

$$C_g(f) = \frac{g}{4\pi f}, \tag{1}$$

where g is the acceleration due to gravity and f is the frequency (Hz). Swell generated at time t_o travel a great-circle distance d and will arrive in time t_a:

$$t_a = t_o + \frac{d}{C_g(f)}. \tag{2}$$

Let O denote the point of wave origin. Differentiation yields an approximate distance between O and the measuring station as given by Earle et al. (1984):

$$\frac{dt_a}{df} = \frac{4\pi d}{g} \approx \left(\frac{t_2 - t_1}{f_2 - f_1}\right), \tag{3}$$

where t_1 and t_2 are the arrival times of swell energy at frequencies f_1 and f_2, respectively. Rearranging and attaching subscripts to denote particular wave measurements at a buoy b, (3) can be rewritten as follows:

$$d_{o,b} \approx \frac{g}{4\pi}\left(\frac{t_{b,f_2} - t_{b,f_1}}{f_{b,2} - f_{b,1}}\right), \tag{4}$$

where $d_{o,b}$ denotes the great-circle distance from O to b, $f_{b,1}$ denotes the frequency of the first swell detected at b, and $t_{b,f1}$ denotes the arrival time of $f_{b,1}$ at b.

Figure 6 shows a schematic diagram of the geometry of the method used to determine the distance and azimuth to O using two buoys. Buoy 1, located at latitude ϕ_1 and longitude λ_1, detects an initial swell of frequency $f_{1,1}$ with an energy density of $E_{1,1}$ at time $t_{1,1}$ and a second wave group of frequency $f_{1,2}$ with a spectral energy density of $E_{1,2}$ at time $t_{1,2}$. Using (4), the distance from O to 1, $d_{o,1}$, can be easily found, and using (1) and (2), t_o can be found. Buoy 2, located at latitude ϕ_2 and longitude λ_2, detects an initial wave group of frequency $f_{2,1}$ with a spectral energy density of $E_{2,1}$ at time $t_{2,1}$, and a second wave group of frequency $f_{2,2}$ with a spectral energy density of $E_{2,2}$ at time $t_{2,2}$.

The swell detected at buoy 1 and buoy 2 can be assumed to have been generated in the same region at the same time if three conditions are met. First, the swell frequencies measured at the buoys must be the same; that is,

$$f_{1,1} = f_{2,1} \quad \text{and} \quad f_{1,2} = f_{2,2}. \tag{5}$$

Second, the order of magnitude of the swell energy, as represented by the spectral energy density at frequencies $f_{1,1}$ and $f_{1,2}$, must be the same; that is,

$$E_{1,1} \approx E_{2,1} \quad \text{and} \quad E_{1,2} \approx E_{2,2}. \tag{6}$$

Finally, the time interval between the initial detection

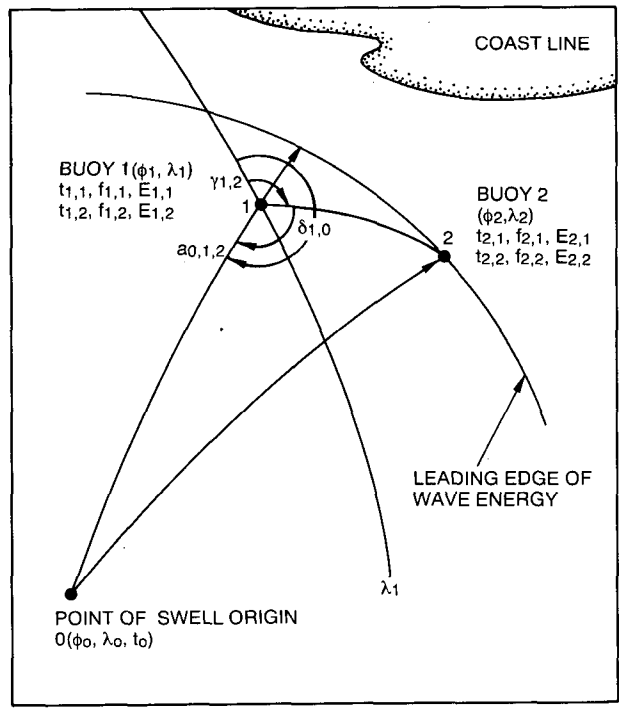

FIG. 6. Diagram of the geometry of the method for determining the source of distant swell from two nondirectional buoys. The necessary measurements are denoted under the headings BUOY 1 and BUOY 2.

of swell at buoy 1 and buoy 2 must be less than or equal to the time it would take that swell energy, traveling at the appropriate frequency-dependent group velocity C_g to travel over the great-circle distance $d_{1,2}$ or

$$t_{2,1} - t_{1,1} \leq \frac{d_{1,2}}{C_g(f_{1,1})}. \quad (7)$$

Locating O requires using variations of the law of sines and the law of cosines for spherical triangles. A spherical earth is assumed. A comprehensive collection of pertinent formulas is given in Snyder (1987). The position of $O(\phi_0, \lambda_0)$ is found using (8) and (9) from Snyder (1987, p. 31), where all single subscripts denote either the buoy identifier b or the swell origin O, where $r_{o,1}$ is the radian measurement of the corresponding great-circle distance $d_{o,1}$, and the angle $\delta_{1,o}$ is the azimuth angle from 1 to O:

$$\phi_o = \sin^{-1}(\sin\phi_1 \cos r_{o,1} + \cos\phi_1 \sin r_{o,1} \cos\delta_{1,o}), \quad (8)$$

$$\lambda_o = \lambda_1 + \tan^{-1}\left(\frac{\sin r_{o,1} \sin\delta_{1,o}}{\cos\phi_1 \cos r_{o,1} - \sin\phi_1 \sin r_{o,1} \cos\delta_{1,o}}\right). \quad (9)$$

To solve (8) and (9), three great-circle distances ($d_{o,1}$, $d_{o,2}$, and $d_{1,2}$) and two angles (the azimuth from 1 to 2, $\gamma_{1,2}$ and the azimuth of O from 1, $\delta_{o,1}$) must be found. The distances $d_{o,1}$ and $d_{o,2}$ are found using (4). The great-circle distance $d_{1,2}$ is found using

$$\sin\left(\frac{r_{1,2}}{2}\right) = \left[\sin^2\left(\frac{\phi_2 - \phi_1}{2}\right) + \cos\phi_1 \cos\phi_2 \sin^2\left(\frac{\lambda_2 - \lambda_1}{2}\right)\right]^{1/2} \quad (10)$$

(Snyder 1987, p. 30), where $r_{1,2}$ is the radian measure of the great-circle distance $d_{1,2}$.

The azimuth angle of O from 1, $\delta_{1,o}$, is found by combining two angles. The first angle, $\alpha_{o,1,2}$, is the internal angle subtended by two great circles—one that extends through 1 and 2, and the other that extends through O and 1. The second angle, $\gamma_{1,2}$, is the azimuth angle from 1 to 2.

The law of cosines can be used to find the angle $\alpha_{o,1,2}$,

$$\alpha_{o,1,2} = \cos^{-1}\left(\frac{\cos r_{o,2} - \cos r_{o,1} \cos r_{1,2}}{\sin r_{o,1} \sin r_{1,2}}\right). \quad (11)$$

Next, the azimuth angle from 1 to 2, $\gamma_{1,2}$, can be found using

$$\tan\gamma_{1,2} = \frac{\cos\phi_2 \sin(\lambda_2 - \lambda_1)}{\cos\phi_1 \sin\phi_2 - \sin\phi_1 \cos\phi_2 \cos(\lambda_2 - \lambda_1)}. \quad (12)$$

The azimuth of O from 1, $\delta_{1,o}$, can be found from (13a) or (13b), such that $\delta_{1,o}$ is either $\delta^+_{1,o}$ or $\delta^-_{1,o}$, and that $\delta^+_{1,o}$ and $\delta^-_{1,o}$ will be equal if $\alpha_{o,1,2}$ is 180°:

$$\delta^+_{1,o} = \gamma_{1,2} + \alpha_{o,1,2}, \quad (13a)$$

$$\delta^-_{1,o} = \gamma_{1,2} - \alpha_{o,1,2}. \quad (13b)$$

The correct azimuth angle $\delta_{1,o}$ can be found by using information from a third buoy. Two possible positions of O, from $\delta^+_{1,o}$ and $\delta^-_{1,o}$ in (8) and (9), can be found from buoy pair 1–2. By substituting a third buoy in place of buoy 2 in (4) through (13), the other two possible positions of O, from $\delta^+_{1,o}$ and $\delta^-_{1,o}$ in (8) and (9), can be found. The third buoy should be in the same region as buoys 1 and 2. The correct azimuth angle will be the one that yields consistent estimates of O from the two buoy pairs, 1–2 and 1–3, when the positions are compared. If a third buoy is unavailable, then the spurious azimuth angle may be eliminated by inspection if the angle points to an unrealistic direction, such as to a wave generation position located over land. For swell coming from the northern portions of the central North Pacific Ocean, the NDBC west coast network of buoys is extensive enough that two and three pairs of buoys can be used to find several azimuth angles to the storm generation area, thereby providing sufficient information to resolve any directional ambiguity.

With knowledge of ϕ_o, λ_o, C_g, and t_o, it is possible to forecast the propagation of the wave energy in time and represent it as a circle on the earth's surface, centered at ϕ_o, λ_o, expanding in time.

6. Determination of wave generation area using nondirectional wave spectra—Case study

Spectral wave estimates from stations 46006, 46002, and 46042 are used to demonstrate the feasibility of using an array of nondirectional buoys to obtain O and t_o. Stations 46006 and 46002 were selected because both are located far offshore. Station 46042 was selected because it provided both directional and nondirectional wave spectra. Each of these stations are located in deep water, so bottom effects should not be significant. The data from stations 46006 and 46002 alone provide sufficient information to produce an accurate estimate of O for manual forecasting purposes. The nondirectional spectral estimates from station 46042 are used to provide information that will resolve the directional ambiguity inherent in the first available buoy pair solution.

Figure 7 shows the time series plots of the 0.05- and 0.06-Hz spectral energy density at stations 46006, 46002, and 46042 from 24 through 28 September. Station 46006 was the first of these three stations to detect long-period swell energy. The 0.05-Hz spectral energy density rose abruptly from less than 0.05 m^2 Hz^{-1} at 1100 UTC 24 September to 10.31 m^2 Hz^{-1} at 1500 UTC. Later, the 0.06-Hz spectral energy density increased rapidly from 9.54 m^2 Hz^{-1} at 0000 UTC 25

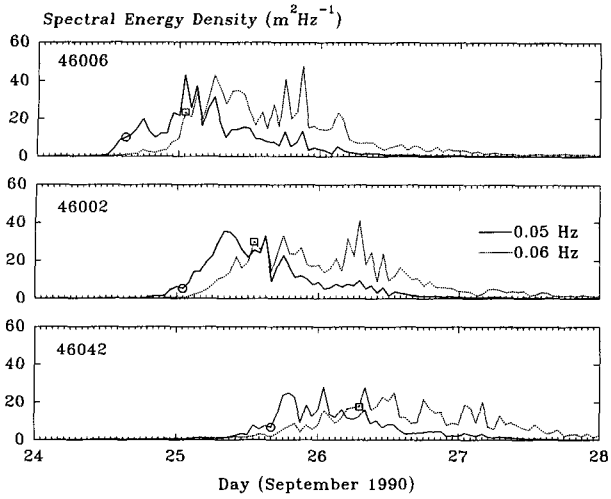

FIG. 7. Time series of 0.05- and 0.06-Hz spectral energy density at stations 46006 (top), 46002 (middle), and 46042 for the period 24–28 September 1990. The circle and square on the curves denote the hours used in the computations.

September to 23.53 m^2 Hz^{-1} 1 h later. From (4), using a time difference, $t_{46006,0.06\text{ Hz}} - t_{46006,0.05\text{ Hz}}$, of 10 h, the source of this swell energy was calculated at a distance $d_{o,46006}$ of approximately 2810 km. Using (2), 0.05-Hz wave energy took approximately 50 h to travel from O to 46006. Thus, t_o was estimated at 1300 UTC 22 September 1990.

The onset of high energy at station 46002 was less abrupt than at station 46006 but still very noticeable. The times 0100 and 1300 UTC 25 September were used for $t_{46002,0.05\text{ Hz}}$ and $t_{46002,0.06\text{ Hz}}$, respectively. Using (4), it was estimated that the distance to the swell origin, $d_{o,46002}$, was approximately 3371 km and that the time of swell origin was again 1300 UTC 22 September. The swell arrival times yield a value of t_o consistent with the estimate made from 46006. It should be noted that the fourth arrival time $t_{46002,0.06\text{ Hz}}$ was not necessary for making an estimate of $d_{o,46002}$. The distance $d_{o,46002}$ was also found from (2) using the value of t_o, estimated from 46006, $t_{46002,0.05\text{ Hz}}$, and C_g(0.05 Hz). For forecasting purposes this method for estimating the general distance $d_{o,2}$ offers a great advantage in time.

The azimuth $\gamma_{46006,46002}$, found by applying the known geographical locations of the stations to (12), was 70.3°. The angle $\alpha_{o,46006,46002}$, found by applying the distances $d_{o,46006}$, $d_{o,46002}$, and $d_{46006,46002}$ to (11), was 148.1°. Two possible bearings to O, $\delta^{+}_{46006,o}$ and $\delta^{-}_{46006,o}$, were 218.4° and 282.2°, respectively. Applying the above results to (8) and (9) gives two positions for O: 19.7°N, 154.0°W and 41.3°N, 171.4°W. The first position may be discounted because it is located approximately 100 km east of the island of Hawaii, an island that could interfere in swell generation.

Energy increased even less rapidly at station 46042 than at 46006 and 46002. The arrival times of 1600 UTC 25 September and 0700 UTC 26 September were used for $t_{46042,.05\text{ Hz}}$ and $t_{46042,.06\text{ Hz}}$, respectively. From (4) it was estimated that $d_{o,46042}$ was 4214 km. The azimuth, $\gamma_{46006,46042}$, was 103.9°, and the angle $\alpha_{o,46006,46042}$ used was 180.0°. Therefore, the *single* possible bearing to O, with $\delta^{+}_{46006,o}$ equal to $\delta^{-}_{46006,o}$, was 283.9°. Applying the above results to (8) and (9) yielded a position for O of 41.9°N, 171.9°W. The values used in the computations did not yield a genuine solution for O because $d_{o,46006}$ plus $d_{46006,46042}$ was less than the calculated value of $d_{o,46042}$, ($d_{46006,46042}$ is 1393.0 km), and the argument of the right side of (11) was slightly greater than unity. However, the difference between the combined distance, $d_{o,46006}$ plus $d_{46006,46042}$, and the distance $d_{o,46042}$, is 11.7 km. Since this distance is less than the distance that a 0.05-Hz wave will travel in the 40 min between NDBC buoy wave data sampling periods, cosine($\alpha_{o,46006,46042}$) was set to unity in succeeding calculations.

Finally, the wave estimates from stations 46002 and 46042 were used to derive a third estimate of O. The values used in the calculations were the same as in the previous two examples. With this information the position of O was found to be either 42.2°N, 171.8°W or 68.5°N, 160.4°W. The results from the 46006–46002, 46006–46042, and 46002–46042 pairs indicate that the wave generation occurred over an area centered near 42°N, 172°W at 1300 UTC 22 September. This result is consistent with the path of the storm.

This method is essentially a process in finding the intersections of two circles on the earth's surface, centered at ϕ_1, λ_1 and ϕ_2, λ_2 with radii $d_{o,1}$ and $d_{o,2}$, respectively. A small error in the identification of any of the swell arrival times used can alter the radius of one of the circles, and a small change in radius can cause very large changes in the intersection positions. The inherent errors in the method can therefore be associated with problems in determining the correct swell arrival times. One source of error comes from the integer hours used for the calculations. NDBC wave estimates are reported once per hour following a 20-min sampling period. If long-period swell energy arrives moments after the sampling period for a particular hour has ended, and the energy continues into the next hour, it will be reported 40 min too late for accurate results. The time errors are compounded with more stations. The problem with the results from the 46006–46042 pair is an example of this kind of error. Also, if the onset of long-period wave energy occurs near the end of the sampling period, there will be lower spectral energy density, preventing the accurate identification of swell energy and resulting in delay and inaccuracy.

No single energy threshold was used in identifying the onset of long-period swell energy in the preceding analyses. The times for $t_{b,f1}$ and $t_{b,f2}$ were found by visual inspection of the time series of spectral energy density. Automating the identification of swell by particular energy thresholds, time rate of change thresh-

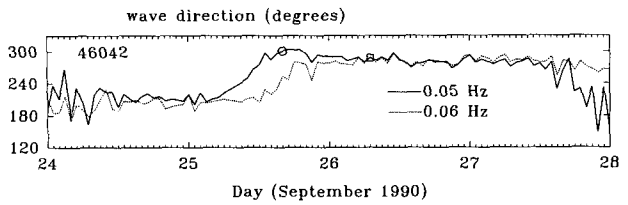

FIG. 8. Time series of the mean wave direction θ_1 of 0.05 and 0.06 Hz for station 46042 from 24 to 28 September 1990.

olds, and other means could be accomplished with further study of individual buoy responses to swell.

7. Determination of wave generation area using directional wave spectra

The directional wave estimates from 46042 were used to estimate O by using t_o, found in section 6, and the mean wave direction of 0.05-Hz wave energy, found from the directional distribution function. Time series plots of θ_1 at 0.05 and 0.06 Hz are shown in Fig. 8. The wave direction of 0.05-Hz swell energy, θ_1, or also, $\delta_{46006,o}$, at $t_{46042,0.05\text{ Hz}}$ was 301°, denoted by o in Fig. 8. This wave direction and the distance $d_{o,46042}$ of 4214 km in (8) and (9) yield a position, 46.5°N, 172.4°W, approximately 590 km north of the positions found using the previous method.

This result agrees fairly well with the three earlier results. Notwithstanding the complexity of wave calculations from a directional buoy, the relative simplicity in obtaining O once the mean wave direction is determined, compared with the previous method, is noted. Current positions of NDBC directional buoys in coastal areas prevent using them for early warning applications. It should be stressed, however, that strategically positioned NDBC directional buoys offer an opportunity for automated swell analysis, forecasting, and warning capability.

8. Determination of wave generation area using the ridge-line method and meteorological analyses

Another method for determining O and t involves using, first, contours of energy density on a time-frequency plot; second, appropriate meteorological charts; and, finally, (1) and (2). Dispersion theory predicts (Munk et al. 1963) that energy peaks associated with swell events will produce slanting ridges that appear as straight lines through the contours of spectral density on a time-frequency plot. The intersection of the ridge line with the $f = 0$ line will give t_o (Cartwright et al. 1977). The onset of swell can be identified by a particular spectral energy density threshold at a frequency f at a time t_a. Equations (1) and (2) can then be used to find the distance to O. Once t_o and $d_{o,b}$ are found, a synoptic weather chart or satellite depiction for the given time, t_o, encompassing the area at the appropriate distance, $d_{o,b}$, can be inspected to find O, an area of high winds over a sufficient fetch.

Figures 9–11 show contour plots of energy density as a function of frequency and time for stations 46006, 46002, and 46042, respectively. The contours are in intervals of one-tenth of the maximum energy density

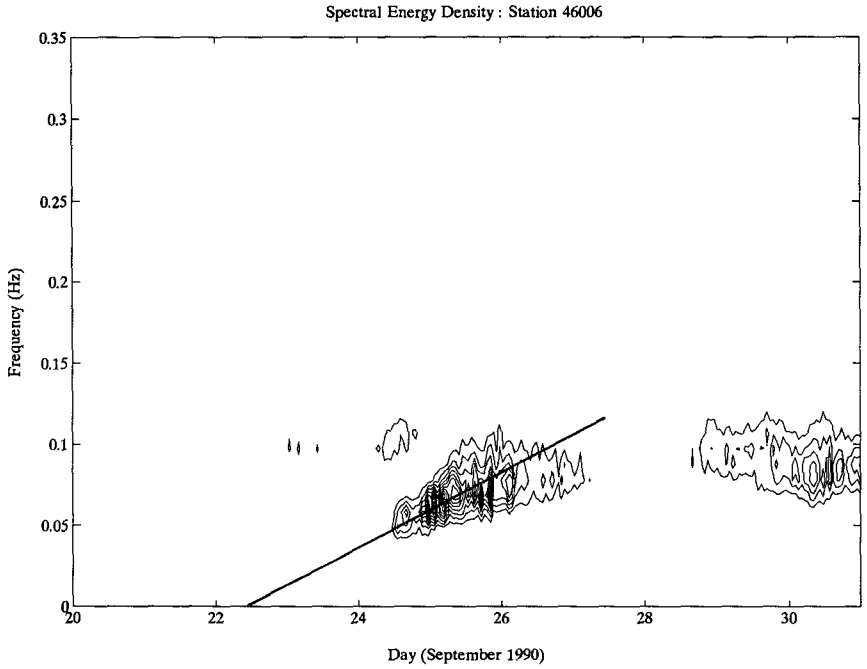

FIG. 9. Contour plot of energy density as a function of frequency and time for station 46006.

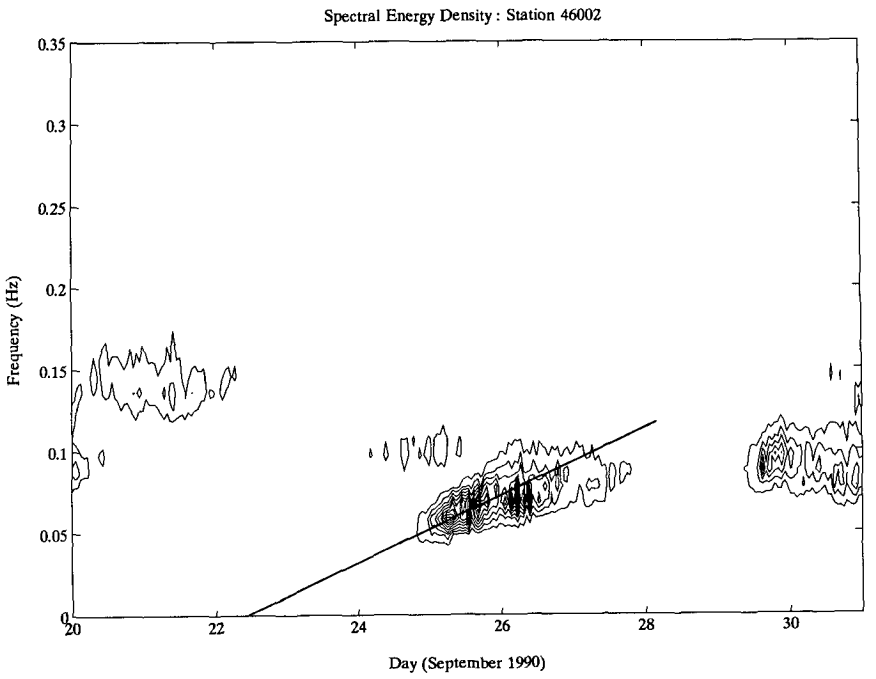

FIG. 10. Contour plot of energy density as a function of frequency and time for station 46002.

measured over the time period shown. The energy maxima at 46006, 46002, and 46042 were 47.83, 41.15, and 28.16 m^2 Hz^{-1}, respectively.

Significant low-frequency energy appeared at 46006 at about 1200 UTC 24 September with an energy packet sloping slightly up to the right and ending at about 0000 UTC 27 September. The onset of 0.05-Hz energy has already been shown to have occurred at 1500 UTC 24 September (Fig. 7). When a line is drawn along the ridge line of the axis of the packet, the in-

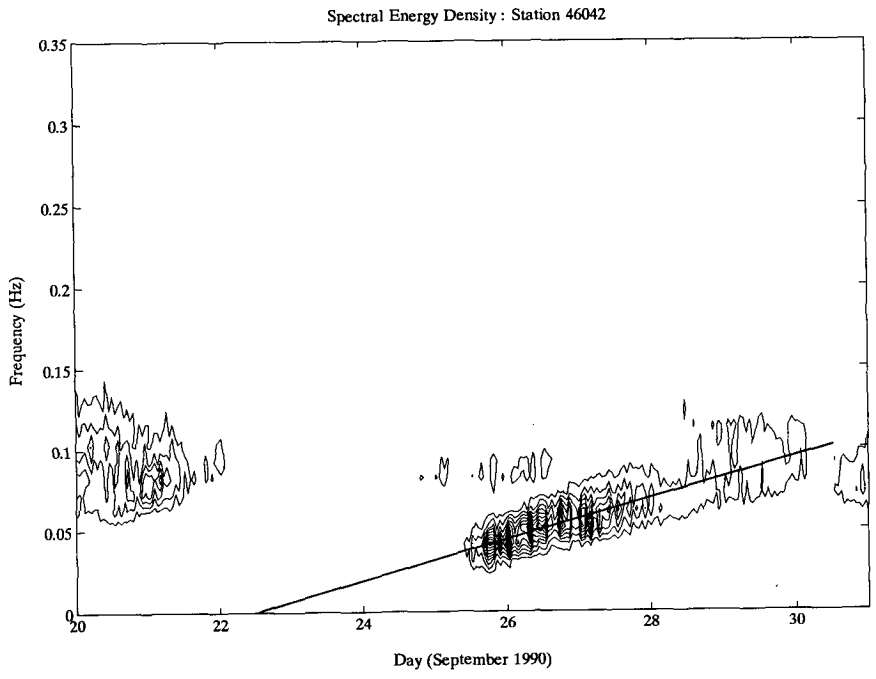

FIG. 11. Contour plot of energy density as a function of frequency and time for station 46042.

tersection of the line with the $f = 0$ axis occurred about 1100 UTC 22 September. The distance $d_{o,1}$ using (1) and (2) was therefore approximately 2922 km, 112 km farther than found in section 6. When this technique is applied in Fig. 10 for 46002, the intersection is also near 1100 UTC 22 September, and when applied in Fig. 11 for 46042, the intersection is about 1200 UTC 22 September.

Figures 12 and 13, the U.S. National Weather Service Pacific Ocean surface pressure analyses for 0000 and 1200 UTC 22 September, show the extratropical remnants of Typhoon Flo. At 0000 UTC the storm was located near 47.5°N, 180.0°, approximately 3410 km from 46006, and had a central pressure of 968 hPa. Two ship reports near the center of the storm reported winds in excess of 25 m s^{-1}. At 1200 UTC the storm was centered near 48.5°N, 171.5°W, approximately 2780 km from 46006 and had a central pressure of 968 hPa. The distance of 46006 to the 1200 UTC position of the storm is within 5% of the distance computed from the ridge-line plots. The pressure field south of the storm indicates that strong westerly geostrophic wind speeds extended in an area from the center of the storm south to about 40°N at 0000 UTC and to about 43°N at 1200 UTC. These figures show the rather broad area over which the swell was generated. It is evident that the swell generation time was not much later than 1200 UTC 22 September and that the swell that affected the west coast buoys was generated in an area near 43°N, 176°W. This time and position are consistent with the results of the previous two methods.

Full use of the ridge-line meteorological analysis method is not a viable method for forecasting purposes. However, a simplified approach using past weather charts and buoy data applied to the wave dispersion relationships given in (1), (2), and (4) (instead of using the full spectral density contour plot) will yield sufficient information for forecasting needs.

9. Determination of wave generation area using the Global Spectral Ocean Wave Model

The results of the above analyses are compared with the estimates of wave height from the GSOWM. Descriptions of the GSOWM are given by Clancy et al. (1986), Zambresky (1987), and Wittmann and Clancy (1991). The GSOWM is a first-generation wave model that is run operationally at FNOC. The model is forced by the winds produced by the Navy Operational Global Atmospheric Forecasting System Prediction model and is run on a 2.5° spherical grid twice per day. GSOWM produces two-dimensional wave spectra up to a forecast time of 72 h with a resolution of 15 frequencies by 24 directions. The initial conditions for these forecasts are provided by carrying the predicted, two-dimensional energy spectra forward in time. Several wave parameters, including significant wave height and dominant wave period, are derived from the spectra.

A detailed description of the physics of the Spectral Ocean Wave Model (SOWM), which also generally applies to the GSOWM, is given by Pierson (1982). The wave growth mechanism is that of Inoue (1967). Wave growth slows as the wave spectrum approaches the Pierson and Moskowitz (1964) full-developed spectrum, which serves as the upper limit on spectral growth. Dissipation of wave energy traveling into the wind is accomplished using an empirical function of wave energy, frequency, and the angle between wind and wave directions. Waves running with the wind are not dissipated. The model advects wave energy along great circle paths at the frequency-dependent group velocity for deep-water waves. The model simulates wave dispersion and conserves wave energy. It is important to note that the model is a deep-ocean model and, therefore, not designed to represent wave characteristics in shallow water.

The GSOWM nowcasts for 1200 UTC September 22 and 0000 UTC September 23 covering the area of the central and eastern North Pacific Ocean are shown in Figs. 14a and 14b. The direction of the dominant wave energy (solid arrows) and the dominant wave period (s) are given at each grid point. Contours of significant wave height are plotted in increments of 0.92 m (3 ft). The maximum wave height found is in Fig. 14a, 13.4 m (44 ft) near 44°N, 176°W, a position very close to that found using the ridge lines and weather charts. The location of maximum wave height can also be considered the generation area of the waves that reached the NDBC buoys 2–3 days later.

10. Discussion

The various estimates of O and t_o are summarized in Table 2. It is obvious that the waves that affected the west coast on 25 September were generated 2 days before by the extratropical remnants of Typhoon Flo. The greatest differences among the various estimates was 5° in latitude, 4° in longitude, and 2 h in time. These differences are not surprising considering the expanse and movement of the storm. There was notable consistency among the various results.

Inspection of the relevant 1200 UTC 22 September surface pressure analyses or wave model analyses at the time present clear evidence that swell were being generated and that those swell would propagate eastward and affect the United States west coast three days later. In this sense the best method for identifying swell generation is by continuously monitoring the weather situation closely for active storms. But, while continuous monitoring of the synoptic situation may provide the earliest estimates of swell generation time and location, this method is not suitable for automation, because it requires the manual synthesis of a significant amount of information. The above results show that both directional and nondirectional instrumented buoys can provide sufficient information for making

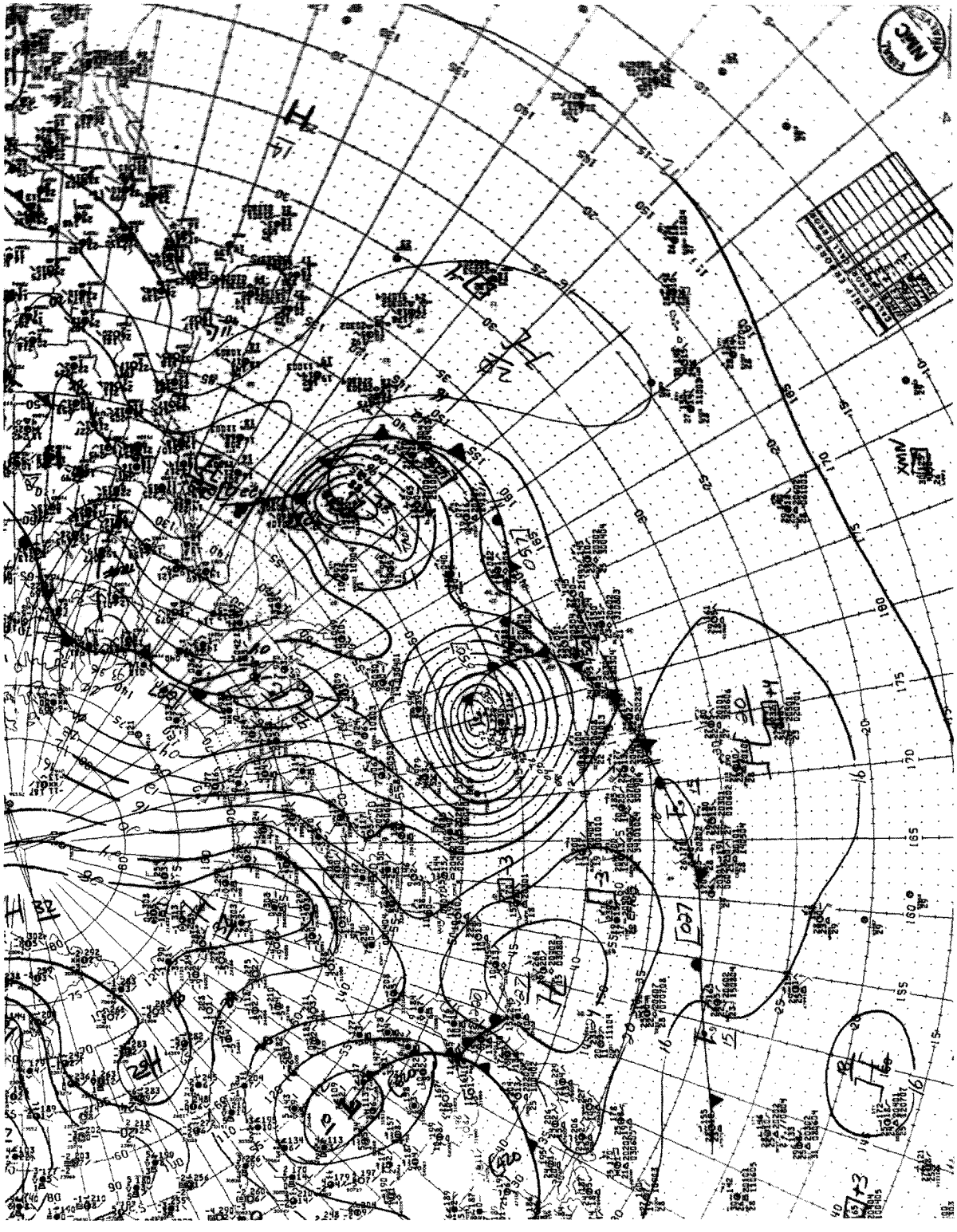

FIG. 12. North Pacific surface synoptic weather chart for 0000 UTC 22 September 1990.

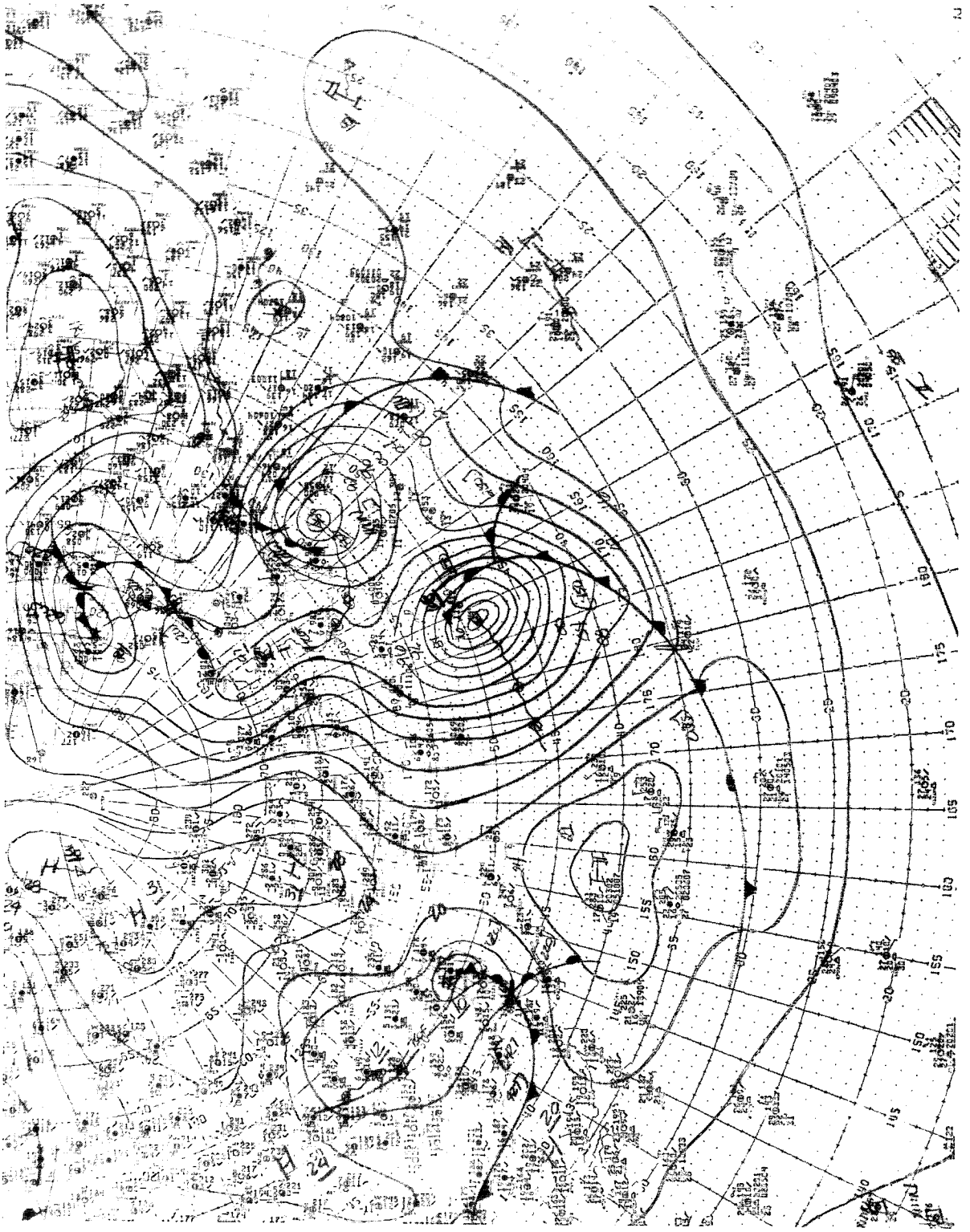

FIG. 13. North Pacific surface synoptic weather chart for 1200 UTC 22 September 1990.

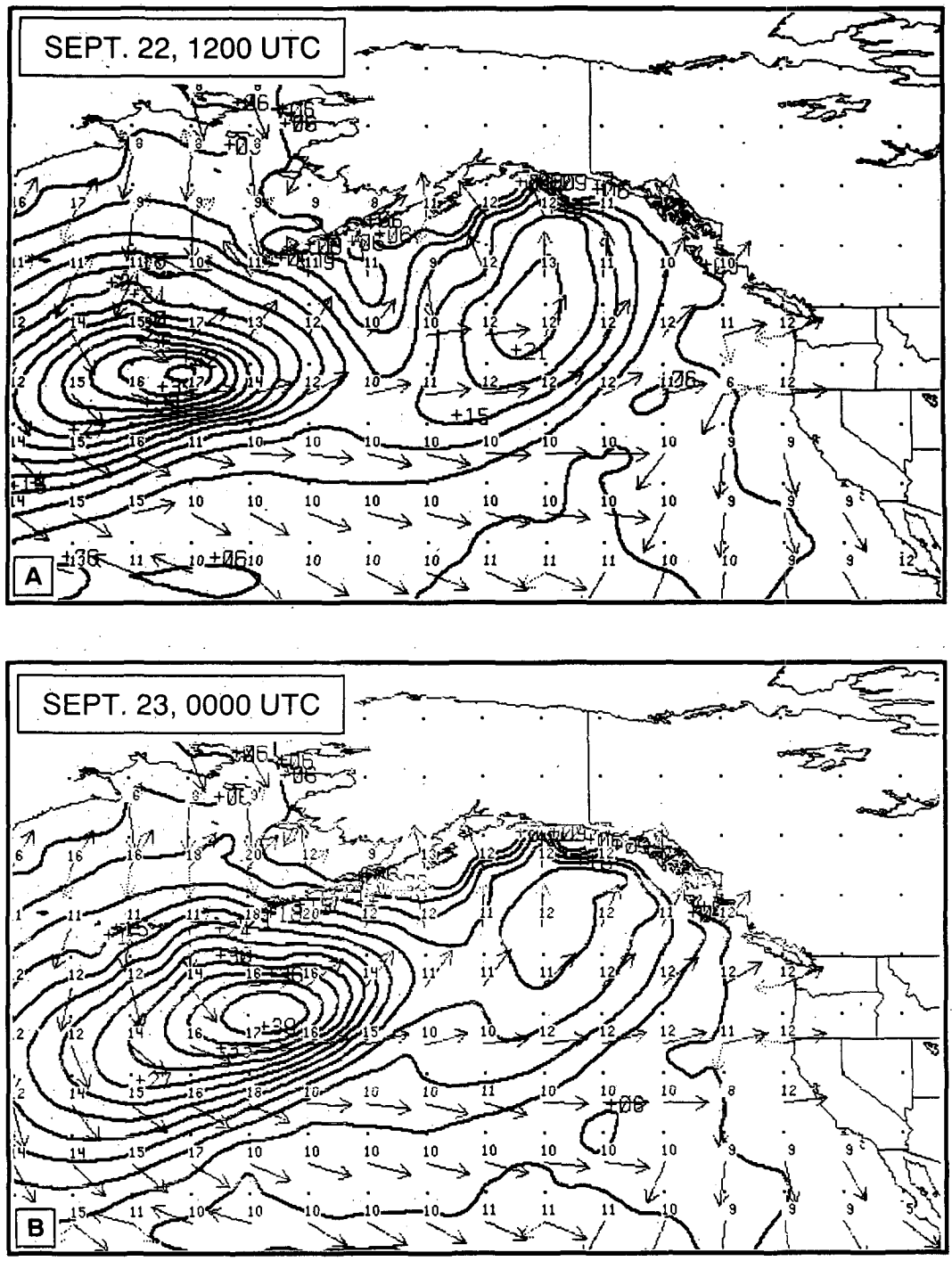

FIG. 14. North Pacific GSOWM nowcasts of significant wave height and dominant wave period for 1200 UTC 22 September and 0000 UTC 23 September 1990.

estimates of swell generation that, while not as timely as current meteorological analyses, are as accurate. Furthermore, in situ observations of swell from buoys can provide invaluable quantitative estimates of energy levels, which are unavailable on surface pressure analyses or wind-forced wave models, such as the GSOWM. Periodic monitoring of nondirectional wave spectra at several fixed locations and of directional wave spectra at a single location provides sufficient information for computerized automated forecasts and warnings.

TABLE 2. Position and time of wave generation.

Method used	O (lat, long)	t_o (UTC) 22 September 1990
46006–46002–46042 (nondirectional stations)	42°N, 172°W	1300
46042 (directional station)	47°N, 172°W	1300
Ridge lines and weather chart	43°N, 176°W	1100–1200
GSOWM	44°N, 176°W	1200

11. Describing the propagation of swell

The propagation of swell from a generation area is assumed to follow linear wave theory. Once O and t_o have been found, it is a simple matter to forecast the propagation of wave energy of frequency f, outward from O as an expanding circle on the earth's surface, increasing in radius, in time, at the frequency-dependent group velocity C_g. An arc of the leading edge of energy of radius d, at any time $t_o + t$, can be described by using (2), (8), and (9), using the appropriate substitutions, for varying values of δ, where δ is redefined as the azimuth from O to a point along the given arc ϕ, λ.

Figure 15 shows the theoretical propagation of 0.05-Hz energy past 16 NDBC buoys on 24 and 25 September. The contours are isochrones of the leading edge of 0.05-Hz energy density based on O and t_o at 42°N, 172°W and 1300 UTC 22 September, respectively, as found from the wave spectra of stations 46006 and 46002 in section 6. The leading edge of 0.05-Hz energy density is defined as the onset of 10 m^2 Hz^{-1} energy density, although the decrease in wave energy with time and distance from generation due to spreading is not accounted for. This energy level is based on the value of $E_{46006,0.05\ Hz}$, 10.31 m^2 Hz^{-1}. All necessary information for forecasting the propagation of the leading edge of the wave energy was available at 0100 UTC 25 September (if the spurious azimuth $\delta^{+}_{46006,o}$ is discounted). Therefore, forecasts of energy arrival time at the coastal buoy stations, 6 h or more in advance, would have been possible.

Figure 16 shows the time series of 0.05-Hz energy density at each of the 14 NDBC west coast stations based on the swell propagation in Fig. 15. The expected arrival time of 0.05-Hz wave energy, with a spectral energy density of 10 m^2 Hz^{-1}, is denoted by the dash-dot vertical line on each plot and an o on the vertical line. These results reveal that both time and energy levels were accurately forecast within 1 h at more than one-half of the stations. The forecasts for 46040, 46027, 46022, 46030, 46014, and 46042 were especially close.

It is interesting to note the marked differences in the energy levels at 46046 and 46010. These stations were only 17 km apart. Station 46046 was located near Cape Disappointment, Washington, and station 46010 is located at the mouth of the Columbia River. The time series plots show that 46046 estimated nearly six times the energy than was estimated by 46010. Also, the time of maximum energy occurred 5 h later at 46010 than at 46046. Neither station was in any way sheltered from incoming wave energy by islands or coastal headlands. Although bottom influences may have been significant, these do not explain why the time of maximum energy at 46010 occurred 5 h later than at 46046. The different responses at these two stations to the incoming swell might be explained by complex wave–current–bathymetry interactions at the Columbia River entrance. Such phenomena have been reported by González (1984).

12. Summary

During 23–25 September 1990, 18 NDBC moored buoy stations measured increased wave heights and dominant wave periods associated with the arrival of long-period swell generated by a far-off storm. Three related, but different, analysis methods were used to determine the time and location of wave generation. Comparison with synoptic weather charts and wave analyses revealed that the swell waves were generated by the 25 m s^{-1} sustained winds associated with the remnants of Supertyphoon Flo in the central North Pacific Ocean during 20–22 September 1990. The swell from the storm radiated outward and reached the West Coast 2–3 days later. There was general agreement among the various methods used to determine the wave generation time and location.

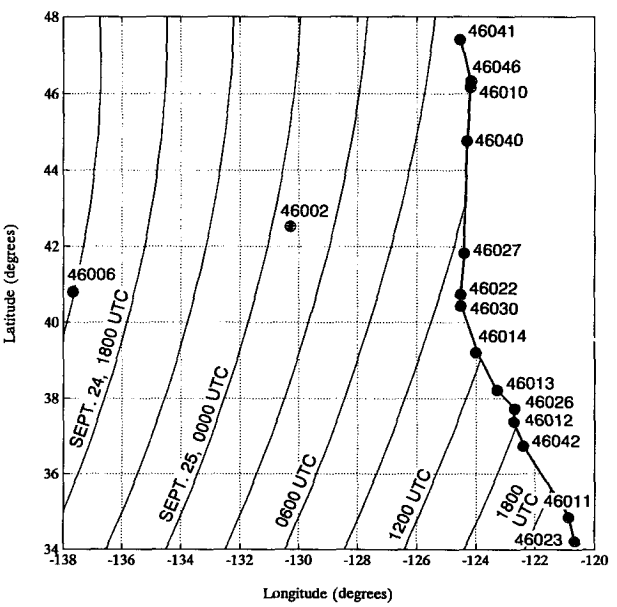

FIG. 15. Propagation of the leading edge of 0.05-Hz 10 m^2 Hz^{-1} wave energy as predicted using information from stations 46006 and 46002.

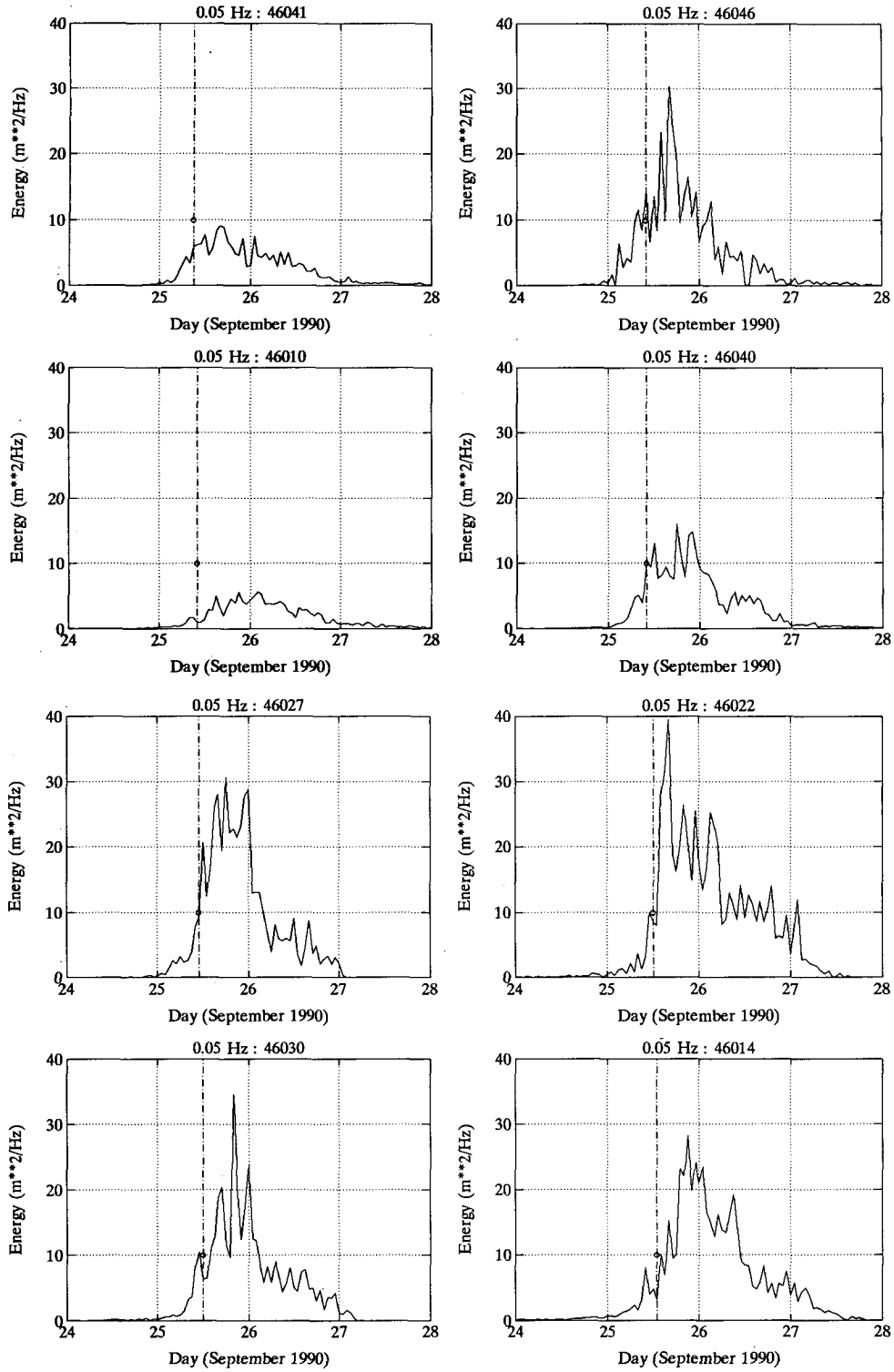

FIG. 16. Time series of 0.05-Hz energy density at 14 coastal stations. The dash–dot vertical line denotes the forecast arrival time for 0.05-Hz energy based on information from nondirectional stations 46006 and 46002. The *o* on each vertical line is the 10 m^2 Hz^{-1} energy level.

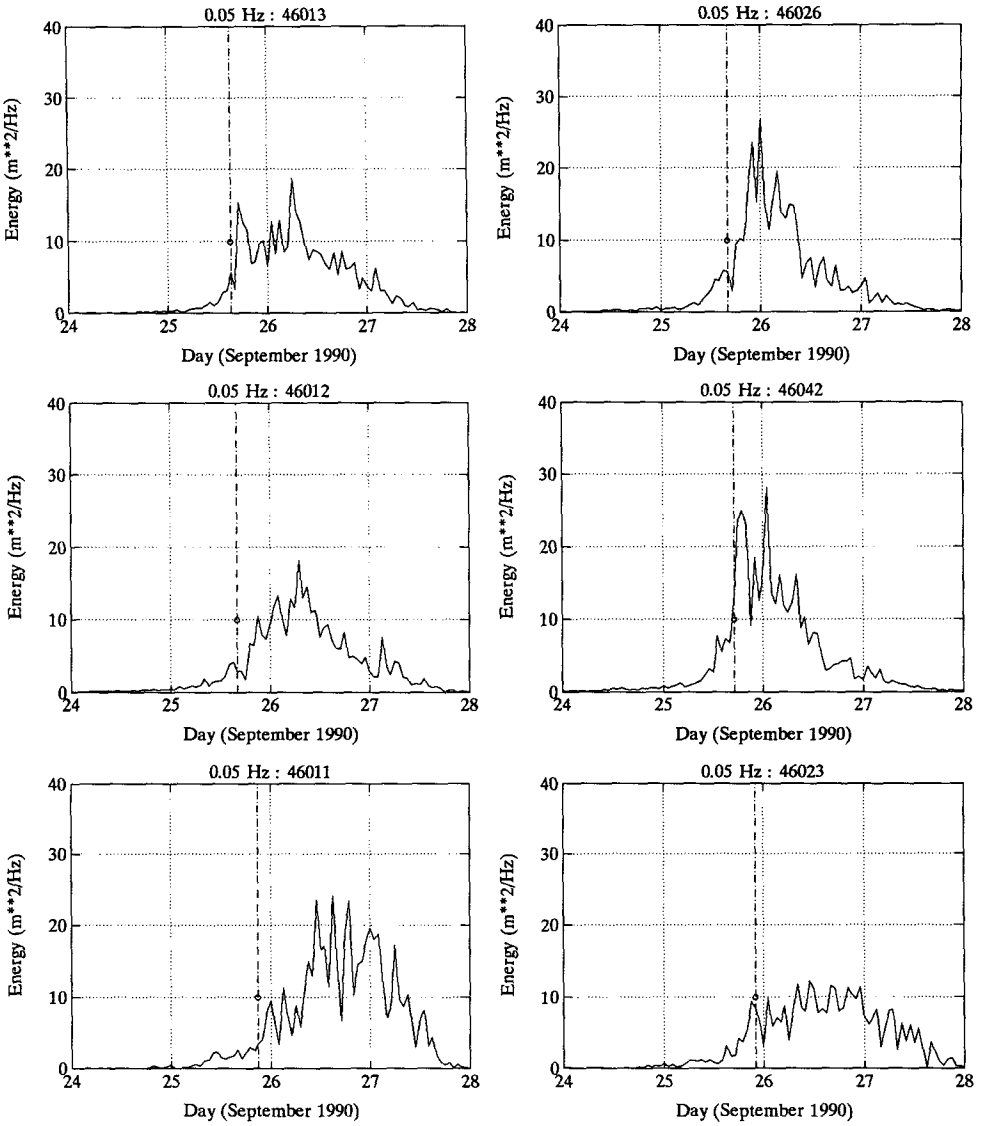

FIG. 16. (*Continued*)

The nondirectional buoy array method used for determining the source of the swell proved to be as accurate as the directional buoy method or the ridge-line method, suggesting that the nondirectional buoy array method can be used interchangeably with the directional buoy method for operational forecasting and data quality control purposes. An important advantage in using a nondirectional buoy array for identifying and forecasting swell is that it can be implemented with currently deployed NDBC buoys. This has been clearly demonstrated in the case of Typhoon Flo. An obvious disadvantage in the nondirectional buoy array method is that more strategically placed buoys must be used than with the directional method. Many more buoys must be used to cover the entire West Coast.

With the assumption that the swell that propagated outward from the remnants of Typhoon Flo traveled in a manner consistent with linear wave theory, the forecasts of the arrival of swell at the coastal buoys, based on the derived swell generation time and location, were accurate to within 1 h at more than half of the 14 buoys. The larger discrepancies in the forecasts may be explained by complex wave–current–bathymetry interactions, such as those that have been found to occur at the mouth of the Columbia River. The differences in the spectral energy density measurements and the times of the peak energy density between stations 46010 and 46046 indicate the need to quantify the quality or the representativeness of the wave estimates from NDBC stations. The simple kinematic model of swell propagation based on data from deep water stations far from shore can be used to find sit-

uations where NDBC buoys do not respond as expected to wave energy because of complex wave–current–bathymetry interactions.

The nondirectional buoy array method is suitable for automation. The communication of all necessary data from buoy to shore occurs fast enough for adequate analysis, and preparation and dissemination of appropriate warnings in advance of the arrival of high swell at the coast. Currently, the nondirectional buoy array method is practicable as a wave warning system only in the case of swell approaching from the northern portions of the central North Pacific Ocean because of the three-ocean-station requirement. There are currently NDBC stations off Washington, Oregon, and California. Since there are only two stations in the Gulf of Alaska and no deep-ocean stations far south of California, there is currently no practical way of implementing the method in these regions. The lack of stations far south of California restricts the ability to forecast the arrival of ocean swell generated by tropical cyclones west of Mexico or by extratropical cyclones in the Southern Ocean. The problem of swell coming in from two or more directions may be solved with added stations, although solutions for such cases are not trivial.

The purpose of this paper has been to demonstrate how wave spectra from NDBC moored buoys can be applied to three related, but different, methods for determining the origin of ocean swell, and thus provide the necessary information to forecast the propagation of that swell. The particular case used to make this demonstration is in many ways ideal, but it does give sufficient evidence to show that automation of swell forecasting procedures is possible. Further improvements to any such forecasting schemes will undoubtedly include improvements to arrival time calculations based on shallow water and current effects.

Acknowledgments. The authors would like to thank Mr. David Gilhousen (NDBC Data Systems) for supporting this study.

REFERENCES

Cartwright, D. E., J. S. Driver, and J. E. Tranter, 1977: Swell waves at Saint Helena related to distant storms. *Quart. J. Roy Meteor. Soc.*, **103,** 655–683.

Clancy, R. M., J. E. Kaitala, and L. F. Zambresky, 1986: The Fleet Numerical Oceanography Center Global Spectral Ocean Wave Model. *Bull. Amer. Meteor. Soc.*, **67,** 498–512.

Earle, M. D., K. A. Bush, and G. D. Hamilton, 1984: Height–height long-period ocean waves generated by a severe storm in the northeast Pacific Ocean during February, 1983. *J. Phys. Oceanogr.*, **14,** 1286–1299.

Gjevik, B., H. E. Krogstad, A. Lygre, and O. Rygg, 1988: Long period swell events on the Norwegian Shelf. *J. Phys. Oceanogr.*, **18,** 724–737.

González, F. I., 1984: A case study of wave–current–bathymetry interactions at the Columbia River entrance. *J. Phys. Oceanogr.*, **14,** 1065–1078.

——, B. M. Holt, and D. G. Tilley, 1987: The age and source of ocean swell observed in hurricane Josephine. *APL Tech. Dig.*, **8,** 94–99.

Hamilton, G. D., 1990: Guide to moored buoys and other ocean data acquisition systems. WMO Report on Marine Science Affairs, No. 16, WMO—No. 750, 57 pp.

——, 1992: Measurement of long-period, low-amplitude swell in the western North Atlantic Ocean. *J. Atmos. Oceanic. Technol.*, **9,** 645–657.

Horrer, P. L., 1948: Southern swell and waves from a tropical storm at Long Beach, California. Wave Report No. 76, 11 pp. [Available from Scripps Institution of Oceanography, University of California, La Jolla, CA 92093.]

Inoue, T., 1967: On the growth of the spectrum of a wind generated sea according to a modified Miles–Philips mechanism and its application to wave forecasting. Tech. Rep. TR-67-5, Geophysical Sciences Laboratory, New York University School of Energy and Science, 66 pp.

Joint Typhoon Warning Center, 1990: 1990 Annual Tropical Cyclone Report. Naval Oceanography Command Center/Joint Typhoon Warning Center, 278 pp. [Available from Commanding Officer, U.S. Naval Oceanography Command Center, COMNAVMARIANAS, Box 12, FPO San Francisco, CA 96630-2926.]

Khandekar, M. L., 1989: *Operational Analysis and Prediction of Ocean Wind Waves.* Springer-Verlag, 214 pp.

Liang, N. K., 1990: A study of typhoon swell height prediction. *Acta Oceanogr. Taiwan.*, **25,** 77–86. (Nai Kuang Liang, Institute of Oceanography, National Taiwan University, Taiwan, Republic of China)

Longuet-Higgins, M. S., D. E. Cartwright, and N. D. Smith, 1963: Observations of the directional spectrum of sea waves using the motion of a floating buoy. *Ocean Wave Spectra,* Prentice-Hall, 111–136.

Munk, W. H., G. R. Miller, F. E. Snodgrass, and N. F. Barber, 1963: Directional recording of swell from distant storms. *Phil. Trans. Roy. Soc. London,* **A255,** 505–584.

Pierson, W. J., 1982: The Spectral Ocean Wave Model (SOWM), a Northern Hemisphere computer model for specifying and forecasting ocean wave spectra. DTNSRDC-82/011, David W. Taylor Naval Ship Research and Development Center, Bethesda, MD, 187 pp.

——, and L. Moskowitz, 1964: A proposed spectral form for the fully developed wind sea based on the similarity theory of Kitaigorodskii. *J. Geophys. Res.*, **69,** 5181–5190.

Snodgrass, F. E., G. W. Groves, K. F. Hasselmann, G. R. Miller, W. H. Munk, and W. H. Powers, 1966: Propagation of ocean swell across the Pacific Ocean. *Phil. Trans. Roy. Soc. London,* **A259,** 430–497.

Snyder, John P., 1987: Map projections—A working manual, U.S. Geological Survey Professional Paper 1395, U.S. GPO, 383 pp. [Available from Superintendent of Documents No.: I 19.16: 1395, U.S. Government Printing Office, Washington D.C. 20402.]

Steele, K. E., and M. D. Earle, 1979: The status of data produced by NDBO Wave Data Analyzer (WDA) systems. *Proc. Oceans '79,* San Diego, CA, Marine Technology Society and IEEE, 212–220.

——, J. Lau, and L. Hsu, 1985: Theory and application of calibration techniques for an NDBC directional wave measurements buoy. *IEEE J. Oceanic Eng.*, **10,** 382–396.

——, C. C. Teng, and D. W. C. Wang, 1992: Wave directional measurements using pitch–roll buoys. *Ocean Eng.*, **19,** 349–375.

Wang, D. W., and R. Carolan, 1991: Estimation of swell direction by a small discus buoy in high seas. Preprints, *Fifth Conf. on Meteorology and Oceanography of the Coastal Zone,* Miami, FL, Amer. Meteor. Soc., 53–59.

Wittmann, P. A., and R. M. Clancy, 1991: Predictions from the GSOWM during LEWEX. *Directional Ocean Wave Spectra,* R. C. Beal, Ed., The Johns Hopkins University Press, 147–151.

Zambresky, L. F., 1987: The operational performance of the Fleet Numerical Oceanography Center Global Spectral Ocean Wave Model. *APL Tech. Dig.*, **8,** 33–36.